THE JOURNAL OF PHYSICAL CHEMISTRY C

Article

Cite This: J. Phys. Chem. C 2019, 123, 22151−22157

pubs.acs.org/JPCC

Role of Dissolution Intermediates in Promoting Oxygen Evolution Reaction at RuO_2(110) Surface

Konstantin Klyukin,[†,#] Alexandra Zagalskaya,[†] and Vitaly Alexandrov*[,†,‡]

[†]Department of Chemical and Biomolecular Engineering and [‡]Nebraska Center for Materials and Nanoscience, University of Nebraska-Lincoln, Lincoln, Nebraska 68588, United States

ABSTRACT: RuO_2 is one of the most active electrocatalysts toward oxygen evolution reaction (OER), but it suffers from rapid dissolution in electrochemical environments. It is also established experimentally that corrosion of metal oxides can, in fact, promote catalytic activity for OER owing to the formation of a surface hydrous amorphous layer. However, the mechanistic interplay between corrosion and OER across metal-oxide catalysts and to what degree these two processes are correlated are still debated. Herein, we employ ab initio molecular dynamics-based blue moon ensemble approach in combination with OER thermodynamic analysis to reveal a clear mechanistic coupling between Ru dissolution and OER at the RuO_2(110)/water interface. Specifically, we demonstrate that (i) dynamic transitions between metastable dissolution intermediates greatly affect catalytic activity toward OER, (ii) dissolution and OER processes share common intermediates with OER promoting Ru detachment from the surface, (iii) the lattice oxygen can be involved in the OER, and (iv) the coupling between different OER intermediates formed at the same Ru site of the metastable dissolution state can lower the theoretical overpotential of OER down to 0.2 eV. Collectively, our findings illustrate the critical role of highly reactive metastable dissolution intermediates in facilitating OER and underscore the need for the incorporation of interfacial reaction dynamics to resolve apparent conflicts between theoretically predicted and experimentally measured OER overpotentials.

INTRODUCTION

Electrochemical water splitting is a promising technology to support renewable hydrogen production.[1−3] Oxygen evolution reaction (OER) is the most energy-intensive part of water splitting thermodynamically as it involves multiple proton-coupled electron transfer steps yielding the Gibbs energy of the overall reaction of water oxidation to molecular oxygen of about 4.92 eV in experiments.[4,5] Noble-metal oxide materials such as RuO_2 and IrO_2 are among the best anode catalysts for OER due to their relatively low overpotentials at practical current densities. The OER process, however, is accompanied by appreciable electrode corrosion in electrochemical environments even for noble-metal-based catalysts. A series of experimental investigations have demonstrated that the activity and stability of many electrocatalysts including Ru, Ir, and Pt are inversely related always requiring a practical compromise between the two.[6−10] Nevertheless, the extent to which these two processes are related is still debated[11,12] due to the lack of mechanistic information on the activity/stability/morphology relationships. For instance, it is still unclear whether OER and catalyst dissolution share common reaction intermediates and how it varies across electrode materials and different facets of nanocatalysts.[13,14] If such atomistic information was available, this would provide strategies to decouple the two processes aiming to increase OER activity with minimal electrode dissolution.

Previous computational density functional theory (DFT)-based studies have provided valuable insights into the thermodynamics of OER for a variety of metal-based catalysts[15−17] including the concept of linear scaling between adsorption energies for OER intermediates.[18] These theoretical investigations have primarily focused on regular defect-free surfaces to compute the thermodynamic overpotential for OER within the computational hydrogen electrode (CHE) approach[18−20] based on the following four-step reaction mechanism (water nucleophilic attack, WNA)

$$* + H_2O \rightarrow HO* + e^- + H^+ \quad (1)$$

$$HO* \rightarrow O* + e^- + H^+ \quad (2)$$

$$H_2O + O* \rightarrow HOO* + e^- + H^+ \quad (3)$$

$$HOO* \rightarrow O_2(g) + e^- + H^+ + * \quad (4)$$

where * denotes the surface active sites and HO*, O*, and HOO* are adsorbed OER intermediates. Each step is characterized by the reaction Gibbs energy ΔG_i (i = 1, 2, 3, 4) with the potential-determining step (PDS) given by

$$\Delta G_{PDS} = \max\{\Delta G_1, \Delta G_2, \Delta G_3, \Delta G_4\} \quad (5)$$

The theoretical overpotential can be then computed as $\eta_{OER} = (\Delta G_{PDS}/e) - 1.23$ V, where 1.23 V corresponds to the equilibrium potential of water splitting. According to this mechanism, the ideal catalyst ($\eta_{OER} = 0$) would have the four equidistant Gibbs free-energy steps of 1.23 eV.

When predicting the OER activity within the DFT-based CHE approach, several key assumptions are typically made. It is assumed that the OER occurs at a single active site following

Received: April 11, 2019
Revised: May 28, 2019
Published: June 7, 2019

DOI: 10.1021/acs.jpcc.9b03418
J. Phys. Chem. C 2019, 123, 22151−22157

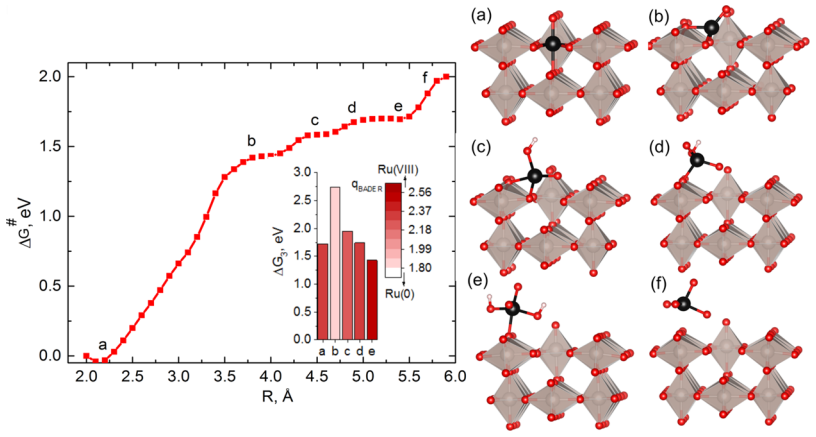

Figure 1. Free-energy profiles ($\Delta G^{\#}$) of Ru dissolution from the $RuO_2(110)$ surface calculated using the AIMD blue moon ensemble approach. (a–f) correspond to the initial, final, and intermediate metastable structures along the dissolution pathway shown on the right panel. Only the top part of the slab is shown with water molecules removed for clarity. The inset shows a relationship between ΔG_3 of the potential-determining step of OER and calculated Bader charges of Ru for all dissolution intermediates (a–e). The final state (f), corresponding to the primary dissolution product $RuO_{4(aq)}$ as detected experimentally, is characterized by the Bader charge of 2.79.

the same reaction mechanism (e.g., WNA) over the catalyst surface that is not being transformed in the course of the reaction. However, there is mounting evidence suggesting a key role of the dynamic evolution of the catalyst/water interface in defining the catalytic activity, reaction mechanisms, and measured OER overpotentials.[21−23] For instance, it was experimentally shown that the formation of amorphous nonstoichiometric oxide layers such as RuO_x and IrO_x, either through the electrochemical oxidation of a metal catalyst or via metal-oxide dissolution, leads to an increased OER performance that gradually decreases upon transformation of the interfacial region into stable RuO_2 and IrO_2.[24−26] This suggests that metastable species formed during electrochemical cycling should be responsible for enhanced OER activity. Indeed, our recent first-principles-based thermodynamic analysis of the OER at Ir surfaces has revealed that thin-oxide precursors formed at the initial stages of Ir surface oxidation should result in improved OER activity relative to both oxidized Ir surfaces and thick-oxide films.[27] It was determined that one of the reasons for such enhanced activity over nonstoichiometric Ir−O layers is the more energetically favorable I2M (interaction of two M−O units) rather than WNA mechanism of OER. These results agree with other theoretical investigations showing that the I2M pathway can be preferred over the WNA mechanism, for example, in the case of β-NiOOH catalyst.[28]

Another important aspect of OER that was not previously addressed computationally is how the OER and dissolution of an electrocatalyst are coupled mechanistically. It was experimentally proposed for a number of noble-metal catalysts such as Ru and Ir that metal corrosion is triggered by OER based on the coincidence of the onsets of OER and dissolution.[14] Based on electrochemical measurements, various possible pathways of metal dissolution during the OER were put forward relating the two processes, but the relationship is not well understood atomistically.[12,14] The main goal of the present computational study is to examine Ru dissolution from the $RuO_2(110)$ surface and determine the OER activity associated with the identified dissolution intermediates. We aim to demonstrate that the OER and corrosion of RuO_2 are coupled processes determining the high OER activity of RuO_2 in electrochemical environments. To this end, we employ ab initio molecular dynamics (AIMD)-based thermodynamic integration calculations to study Ru dissolution and thermodynamic analysis within the CHE approach to investigate the OER on the observed Ru dissolution intermediates. Previously, these approaches were broadly applied to explore the kinetics of transition-metal dissolution (by AIMD) and the thermodynamics of water-splitting reactions (by ab initio thermodynamics) across a variety of oxide systems. In this study, we combine both techniques to investigate the coupling between OER and Ru dissolution at the $RuO_2(110)$ surface.

COMPUTATIONAL METHODOLOGY

Electronic structure calculations are performed within the density function theory (DFT), as implemented in the Vienna ab initio simulation package (VASP).[29,30] We employ the revised Perdew−Burke−Ernzerhof (revPBE) functional[31,32] along with the projected-augmented wave formalism[33,34] and Grimme's D3-dispersion correction[35,36] to incorporate long-range van der Waals interactions. The revPBE exchange−correlation functional was previously shown to provide overpotentials and adsorption energies in good agreement with experimental data.[18,37] The Ru_pv potential is used to include p semicore states as valence electrons for Ru, whereas the standard potentials are chosen for O and H atoms. The energy cutoff of the plane wave basis set of 400 eV is applied, and the convergence criteria for the energy and forces are set to 10^{-6} eV and 0.02 eV/Å during structural optimization, respectively.

AIMD-based simulations are performed to model dissolution of Ru from the $RuO_2(110)$ surface. A periodic slab comprised of four RuO_2 layers with a surface cell of 12.85 × 9.42 Å^2 and a vacuum layer of 8 Å filled with 27 water molecules to provide a water density of about 1 g/cm^3 is used to simulate the $RuO_2(110)$/water interface. To determine the mechanism of Ru dissolution, we first apply DFT-based Born−Oppenheimer molecular dynamics simulations coupled with the slow-growth approach. We use the distance between surface Ru and subsurface O as a collective variable to push Ru to the adsorbed state with a velocity of 0.5 Å/ps determining the sequence of Ru−O bond-breaking events. Then, an accurate evaluation of free-energy barriers ($\Delta G^{\#}$) between intermediate states along the identified Ru dissolution pathway (see Figure 1) is performed using the thermodynamic

DOI: 10.1021/acs.jpcc.9b03418
J. Phys. Chem. C 2019, 123, 22151−22157

integration approach within the blue moon ensemble method, as incorporated into the VASP code.[38] Similar approaches to investigate transition-metal dissolution from nonelectrified oxide surfaces into aqueous solutions have been recently employed in a series of first-principles studies.[39−42] Each configuration shown in Figure 1 is equilibrated for 2 ps, after which the force averaging is done over a 2 ps time frame. A time step of 1.0 fs and the H mass of 3 amu are set in AIMD simulations. The Nose−Hoover thermostat is used to keep the simulation temperature around 300 K. All AIMD calculations are carried out at the Γ point with no symmetry imposed.

To compute OER overpotentials, we apply ab initio thermodynamics within the computational hydrogen electrode (CHE) approach.[18,19] In these calculations, the bottom layer of the slab is fixed to the bulk position, whereas the top three layers are allowed to relax. Simulations are performed using a 3 × 4 × 1 Monkhorst−Pack mesh to sample the Brillouin zone. The Gibbs free energy (ΔG) for OER is obtained by including zero-point energy (ZPE) and entropic contributions ($\Delta G = E$ + ZPE − TS). To estimate the electric potential of the RuO_2 slab, we calculate the work function (Φ) using the Fermi energy level (E_F) and electrostatic potential in vacuum (E_{vac}) as $\Phi = E_F - E_{vac}$ employing the continuum solvation model as implemented in the VASPsol code.[43] The Bader charge analysis[44] is used to determine the evolution of the Ru oxidation state upon dissolution.

RESULTS AND DISCUSSION

Since first-principles simulations cannot realistically cover a diverse set of all possible active sites that may form under real OER conditions at the RuO_2 surface, we illustrate the relation between dissolution and OER by analyzing two representative types of OER active sites. First, we carry out AIMD-based slow-growth calculations in combination with the blue moon ensemble modeling to explore the minimum energy pathway of Ru dissolution from the ideal $RuO_2(110)$ surface. This allows us to identify energetically preferred metastable dissolution intermediates adsorbed at the model surface for which the detailed ab initio thermodynamic analysis of the OER is subsequently performed. The obtained results are then compared to the OER activity of the RuO_2 surface kink that was previously suggested to form during dissolution. Because active Ru dissolution occurs at electrode potentials above 1.23 V, here we focus on the fully oxidized $RuO_2(110)$ surface. The electric potential of the simulated surface referenced to the standard hydrogen electrode (SHE) can be computed as $V_{SHE} = (-4.6 - \Phi)/e$, where Φ is the work function of the slab and −4.6 eV is the approximate chemical potential of SHE.[45] Using the implicit water model with the fully oxidized $RuO_2(110)$ surface, we estimate V_{SHE} to be around 1.96 V. We also determine that V_{SHE} does not change significantly during Ru dissolution evaluated at 1.81 V for the dissolved surface-bound dissolution intermediate. We note, however, that the exact value of the electrode potential is not that important for our purposes since we are not studying how the activation barrier of Ru dissolution varies as a function of the applied potential.

Our AIMD simulations of Ru dissolution from the RuO_2 surface into the aqueous solution reveal that the process proceeds through a number of metastable states, as depicted in Figure 1. Starting from the initial state a in which Ru is 6-fold coordinated by structural oxygen atoms, Ru eventually dissolves as an aqueous RuO_4 complex (state f). The first dissolution step (from state a to b) with an activation barrier of about 1.34 eV is comprised of almost simultaneous breaking of the three structural Ru−O bonds followed by the formation of a bond between the dissolving Ru ion and an adjacent bridging oxygen atom. Upon breaking of the next Ru−O bond, a H_2O molecule from the solution attacks dissolving Ru to yield an OH group with an activation barrier of 0.25 eV (state c). During the next step, one more bond between Ru and surface O becomes broken accompanied by deprotonation of the newly formed OH group and attachment of H_2O from the solution, which subsequently dissociates to yield OH bound to dissolving Ru (state d). For this reaction step, we have also observed in simulations that instead of water nucleophilic attack to compensate for the broken structural Ru−O bond described above, dissolving Ru can alternatively snatch the other nearest structural oxygen atom. This can explain the experimentally observed leaching of the lattice oxygen during dissolution,[23] which may further promote Ru dissolution due to the formation of short-lived oxygen vacancies. For the next dissolution step (from state d to e), after a short period of time, another H_2O from the solution attacks the dissolving Ru ion to form the second OH group. These last two steps require the activation barriers of 0.09 and 0.20 eV, correspondingly. It should be pointed out that under real electrochemical conditions, dissolution barriers should be some functions of the electrode potential applied to drive OER. Nevertheless, the qualitative picture of the dissolution mechanism along with its coupling to OER should be captured in our simulation model, as discussed below.

We next demonstrate using the identified dissolution intermediates that Ru dissolution and OER are coupled processes sharing a set of common reaction intermediates. Also, the computed overpotential of OER turns out to be considerably lower for the surface-bound dissolution intermediate than for regular RuO_2 surfaces. According to the simulated dissolution mechanism (Figure 1), interfacial transformations involve a series of bond-breaking and bond-forming events including dissociation of water molecules, which is the initial step in OER (step 1). The formation of OOH intermediate (step 3) is known to be the potential- and rate-determining step for OER at the pristine $RuO_2(110)$ surface with the reaction Gibbs free energy ΔG_3 of 1.72 eV, as calculated in our work (see the bar plot inset in Figure 1). Here, we show that the formation of OOH species should be even more thermodynamically unfavorable with the energy steps of 2.84 and 1.95 eV at the initial stage of dissolution (the bars b and c in Figure 1). Being unsaturated, Ru has a potential to increase the oxidation state and recover coordination with oxygen, either structural or from solution H_2O. Thus, it is energetically more favorable to bind an additional H_2O molecule rather than to loose O due to the formation of OOH and O_2 species. The formation of OOH intermediate at the dissolving Ru site for states d and e is characterized by the decreased thermodynamic steps of 1.79 and 1.43 eV, respectively. Thus, although the initial steps of Ru dissolution promote water dissociation, the formation of OOH and O_2 species become energetically more favorable at the final steps of dissolution. The final dissolution intermediate bound to the surface (state e) renders the overpotential for step 3 of OER of only 0.2 eV suggesting that such intermediates should outperform the most active sites identified in previous theoretical studies of RuO_2[20,37,46] being in agreement with experimental data for OER on RuO_2.[47] The Bader charge analysis shows that the oxidation state of dissolving Ru

DOI: 10.1021/acs.jpcc.9b03418
J. Phys. Chem. C 2019, 123, 22151−22157

gradually increases approaching the Bader charge of 2.79 for the completely dissolved $RuO_{4(aq)}$ species, which correlates well with the decrease in ΔG_3.

The dissolution intermediates found in our simulations have several OH/O groups exposed to the solution, as seen in Figure 1. For the flat rutile-structured surfaces, such as $RuO_2(110)$, it is typical to analyze the energetics of OER occurring at a single reaction site. However, the presence of several reactive sites at the same interfacial Ru center of dissolution intermediates may imply coupling between OER reaction intermediates since their nature greatly affects the charge state of Ru. Therefore, we next analyze the influence of possible cooperativity between several OER intermediates on the OER energetics. We first focus on the $RuO_2(OH)_2$ dissolution intermediate at the $RuO_2(110)$ surface (state e), which gives rise to the lowest theoretical overpotential of the potential-limiting step (ΔG_3) and compute the thermodynamics of the four-step OER process. In particular, we look at the coupling between OER intermediates at the equatorial (top reaction) and axial (side reaction) active sites as an example.

It is seen from the two-dimensional matrix in Figure 2 that the coupling between two OER reactions should significantly

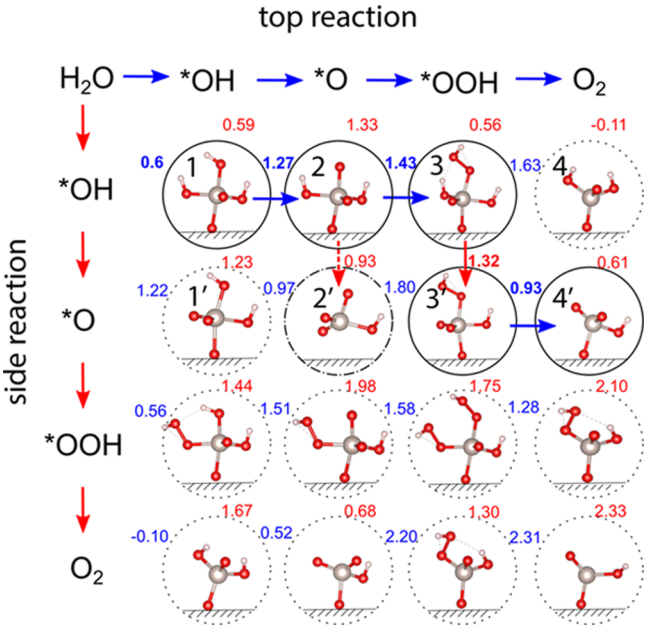

Figure 2. Reaction Gibbs free energies ΔG for the two coupled OERs occurring on top (blue numbers) and side (red numbers) oxygen sites of the Ru dissolution intermediate e. The most energetically favorable pathways for OER (1−2−3−3′−4′) and dissolution (1−2−2′) are highlighted. Pathways 1−4 and 1′−4′ correspond to OER on the top of Ru with OH or O on the side.

affect the overall reaction pathway by changing the thermodynamic heights of the reaction steps. Specifically, we observe that the most thermodynamically favorable pathway is 1−2−2′, where state 1 corresponds to the $RuO_2(OH)_2$ dissolution intermediate, leading to the detachment of Ru as RuO_3OH with an overpotential of only 0.04 eV based on our thermodynamic estimate. When this detached species is placed into an aqueous solution, we observe after a short equilibration time that RuO_3OH deprotonates to form $RuO_{4(aq)}$. We note that the formation of the RuO_3OH intermediate upon RuO_2 dissolution during OER was indeed proposed based on the experimental data as a step preceding the formation of dissolved $RuO_{4(aq)}$.[14,47,48] The other favorable reaction pathway involving $RuO_2(OH)_2$ (1−2−3−3′−4′) leads to OER characterized by a small theoretical overpotential of 0.2 eV. We also want to point out that coupling between multiple reactions is linked to the charge state of Ru, as demonstrated by the Bader change analysis. In particular, the removal of a proton during the side reaction 3−3′ increases the effective charge on Ru and leads to destabilization of OOH intermediate atop of Ru and, thus, promotes OER. Projected density of states for reaction intermediates 3 and 3′ also shows that this destabilization is associated with increased occupancy of the antibonding orbitals formed upon hybridization of the Ru 4d and O 2p states.

We point out that the surface-bound dissolution intermediates found in our simulations bear close similarities with a structural motif of the stable reconstructions of the (110)-RuO_2 surface determined recently by using first-principles evolutionary algorithm search.[49] The identified surface atomic structures characterized by multiple Ru−O bonds exposed to the solution were also found to be stable at elevated temperatures with dynamical changes of O−Ru−O angles in AIMD simulations. To further demonstrate that our conclusions about the coupling between several OER at the same reaction site are not limited to the dissolution intermediates obtained from AIMD calculations for Ru detachment from the flat surface, we also examine the kink active site that may form at $RuO_2(110)$ during the dissolution. The dissolution process from such kink sites should clearly be characterized by reduced activation energies compared to the flat $RuO_2(110)$ surface. Various types of kink motifs at the RuO_2 surface were previously examined computationally,[46] and here we focus on the bridge-CUS (coordinatively undersaturated site) double kink (see Figure 3) characterized by the presence of two O atoms (O_s and O_t) exposed to the solution, and thus we can also explore the coupling between two OER at the same site. Figure 3 shows the atomic structure of the kink with the estimated thermodynamics for all four elementary steps for two coupled OER. It is seen that the most favorable reaction pathway corresponds to the case when one O_sH deprotonates to form O_s, whereas the reaction at the O_t site proceeds with the highest theoretical overpotential of 0.35 eV.

The computational results presented thus far allow us to link Ru dissolution and OER at the $RuO_2(110)$ surface at the mechanistic level, as shown in Figure 4. First steps of dissolution are associated with several bond-breaking events and nucleophilic water attacks leading to the oxidation of Ru(IV) to Ru(VI) and the formation of the surface-bound $RuO_2(OH)_2$ oxyhydroxide complex in accordance with the previous experimental hypothesis.[48,50,51] The formed complex is attached to the surface through the oxygen atom and could either dissolve as RuO_4 (see corrosion cycle in Figure 4) or participate in OER (see OER cycle in Figure 4). As discussed above, the most energetically favorable oxygen evolution pathway exhibits a significantly lower overpotential for the potential-limiting step of OER than the kink and flat surfaces of $RuO_2(110)$ (0.2 vs 0.35 vs 0.52 eV). It also shows that the dissolution of Ru is even more energetically favorable for this specific dissolution intermediate, however, other metastable surface states may have different energetic relationships between OER and dissolution, thereby affecting the balance

DOI: 10.1021/acs.jpcc.9b03418
J. Phys. Chem. C 2019, 123, 22151−22157

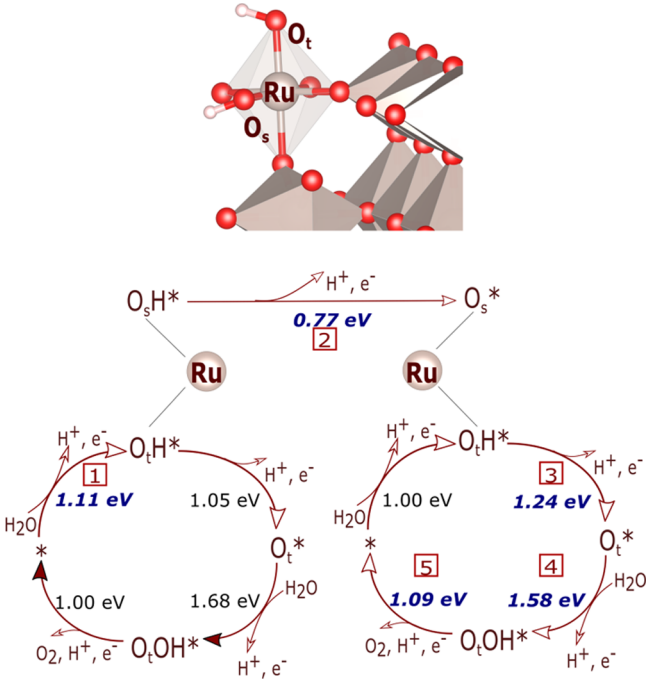

Figure 3. Reaction Gibbs free energies ΔG for the two coupled OERs occurring at the double kink surface of RuO_2 taken from ref 46. Oxygen atoms on the top and side of Ru are labeled as O_t and O_s, correspondingly. The most energetically favorable pathway is highlighted in bold.

between the loss of material and turnover frequency of the catalyst.

CONCLUSIONS

In this work, we have investigated the interplay between OER and Ru dissolution at the $RuO_2(110)$ surface by elucidating the mechanistic details of how these processes are coupled at the atomic scale. Our simulations demonstrate that the formation of metastable Ru dissolution intermediates adsorbed at the surface results in the theoretical OER overpotential as low as 0.2 eV. This helps explain the highly active nature of RuO_2 toward OER including the case of electrochemically activated nanocatalysts. The obtained results are in agreement with previous experimental studies[14,47,48] showing that the onset of OER and dissolution coincide well for RuO_2 and suggesting that the dissolution is triggered by OER.

The study qualitatively confirms the experimentally proposed reaction mechanism involving the oxidation of a surface-bound $RuO_2(OH)_2$ dissolution intermediate via RuO_3OH into $RuO_{4(aq)}$. It is also observed in simulations that the dissolving Ru species may be stabilized at the surface not only by splitting water but also by snatching lattice oxygen that will evolve into oxygen molecules as a result of OER, in agreement with experimental observations[21,52] and thermodynamic arguments.[11] We also demonstrate that the coupling between different OER intermediates at the same catalytic site of the electrode surface can modify the overall reaction pathway and energetics, an aspect previously disregarded in theoretical studies of OER. It should be stressed that under real electrochemical conditions, a range of metastable catalytically active Ru intermediates could be realizable leading to a complex dependence of the macroscopically measured OER overpotentials. Thus, an accurate quantitative comparison between theoretical predictions and experimental values is challenging and would ideally require an evaluation of steady-state concentrations of catalytically active sites as well as activation barriers for the coupled OER and dissolution processes.

Overall, the obtained mechanistic insights should help advance the development of more corrosion resistant materials with high catalytic activity. For example, we can envision the development of a layered oxide material utilizing the highly reactive nature of metastable Ru−O species strongly attached to a support to suppress materials dissolution. Recent experiments have indeed demonstrated the power of corrosion engineering for transforming metal-oxide catalysts into highly active and stable electrodes for OER.[53] Since we do observe the involvement of lattice oxygen in OER upon Ru dissolution,

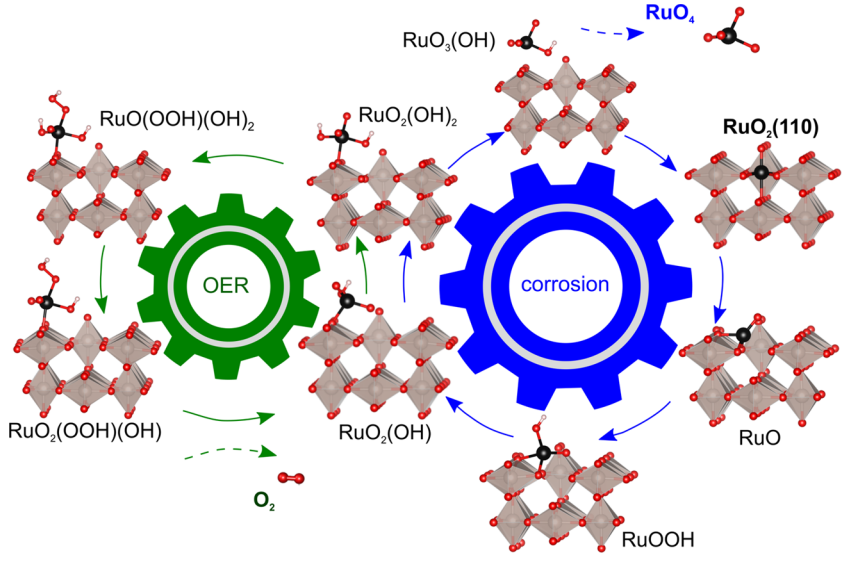

Figure 4. Schematic representation of the found coupling between corrosion and oxygen evolution reaction for the representative dissolution intermediate determined in AIMD simulations for the $RuO_2(110)$ surface. Dissolution and OER cycles are highlighted in blue and green, respectively.

DOI: 10.1021/acs.jpcc.9b03418
J. Phys. Chem. C 2019, 123, 22151−22157

developing chemistries that would minimize oxygen-ion diffusion without sacrificing the electric conductivity, as previously proposed,[11] would be a feasible strategy. In addition, we suggest that future computational-based rational design of electrocatalysts, if it is aimed to capture both the activity and stability of the electrode in dynamic electrochemical environments, should involve descriptors accounting for the transient nature of electrocatalyst/water interfaces rather than relying on a single static-property descriptor.

AUTHOR INFORMATION

Corresponding Author

*E-mail: valexandrov2@unl.edu. Phone: +1 402 4725323.

ORCID

Konstantin Klyukin: 0000-0001-8325-8725

Vitaly Alexandrov: 0000-0003-2063-6914

Present Address

#Department of Materials Science and Engineering, Massachusetts Institute of Technology, 77 Massachusetts Avenue, Cambridge, MA, 02139, United States.

Notes

The authors declare no competing financial interest.

ACKNOWLEDGMENTS

This research used resources of the National Energy Research Scientific Computing Center, a DOE Office of Science User Facility supported by the Office of Science of the U.S. Department of Energy under Contract No. DE-AC02-05CH11231. This research has been partially supported by the American Chemical Society, Petroleum Research Fund (ACS PRF 58410-DNI5).

REFERENCES

(1) Cook, T. R.; Dogutan, D. K.; Reece, S. Y.; Surendranath, Y.; Teets, T. S.; Nocera, D. G. Solar energy supply and storage for the legacy and nonlegacy worlds. *Chem. Rev.* **2010**, *110*, 6474−6502.

(2) Walter, M. G.; Warren, E. L.; McKone, J. R.; Boettcher, S. W.; Mi, Q.; Santori, E. A.; Lewis, N. S. Solar water splitting cells. *Chem. Rev.* **2010**, *110*, 6446−6473.

(3) Gahleitner, G. Hydrogen from renewable electricity: An international review of power-to-gas pilot plants for stationary applications. *Int. J. Hydrogen Energy* **2013**, *38*, 2039−2061.

(4) Over, H. Surface chemistry of ruthenium dioxide in heterogeneous catalysis and electrocatalysis: from fundamental to applied research. *Chem. Rev.* **2012**, *112*, 3356−3426.

(5) Oberhofer, H. *Handbook of Materials Modeling: Applications: Current and Emerging Materials*; Andreoni, W.; Yip, S., Eds.; Springer International Publishing: Cham, 2018; pp 1−33.

(6) Reier, T.; Oezaslan, M.; Strasser, P. Electrocatalytic oxygen evolution reaction (OER) on Ru, Ir, and Pt catalysts: a comparative study of nanoparticles and bulk materials. *ACS Catal.* **2012**, *2*, 1765−1772.

(7) Cherevko, S.; Zeradjanin, A. R.; Topalov, A. A.; Kulyk, N.; Katsounaros, I.; Mayrhofer, K. J. Dissolution of noble metals during oxygen evolution in acidic media. *ChemCatChem* **2014**, *6*, 2219−2223.

(8) Cherevko, S.; Geiger, S.; Kasian, O.; Kulyk, N.; Grote, J.-P.; Savan, A.; Shrestha, B. R.; Merzlikin, S.; Breitbach, B.; Ludwig, A.; et al. Oxygen and hydrogen evolution reactions on Ru, RuO_2, Ir, and IrO_2 thin film electrodes in acidic and alkaline electrolytes: A comparative study on activity and stability. *Catal. Today* **2016**, *262*, 170−180.

(9) Danilovic, N.; Subbaraman, R.; Chang, K.-C.; Chang, S. H.; Kang, Y. J.; Snyder, J.; Paulikas, A. P.; Strmcnik, D.; Kim, Y.-T.; Myers, D.; et al. Activity-stability trends for the oxygen evolution reaction on monometallic oxides in acidic environments. *J. Phys. Chem. Lett.* **2014**, *5*, 2474−2478.

(10) Stamenkovic, V. R.; Strmcnik, D.; Lopes, P. P.; Markovic, N. M. Energy and fuels from electrochemical interfaces. *Nat. Mater.* **2017**, *16*, 57.

(11) Binninger, T.; Mohamed, R.; Waltar, K.; Fabbri, E.; Levecque, P.; Kötz, R.; Schmidt, T. J. Thermodynamic explanation of the universal correlation between oxygen evolution activity and corrosion of oxide catalysts. *Sci. Rep.* **2015**, *5*, No. 12167.

(12) Kasian, O.; Grote, J.-P.; Geiger, S.; Cherevko, S.; Mayrhofer, K. J. The common intermediates of oxygen evolution and dissolution reactions during water electrolysis on iridium. *Angew. Chem., Int. Ed.* **2018**, *57*, 2488−2491.

(13) Roy, C.; Rao, R. R.; Stoerzinger, K. A.; Hwang, J.; Rossmeisl, J.; Chorkendorff, I.; Shao-Horn, Y.; Stephens, I. E. Trends in activity and dissolution on RuO_2 under oxygen rvolution conditions: particles versus well-defined extended surfaces. *ACS Energy Lett.* **2018**, *3*, 2045−2051.

(14) Cherevko, S. Stability and dissolution of electrocatalysts: Building the bridge between model and real world systems. *Curr. Opin. Electrochem.* **2018**, *8*, 118−125.

(15) Gu, Z.; Balbuena, P. B. Dissolution of oxygen reduction electrocatalysts in an acidic environment: Density functional theory study. *J. Phys. Chem. A* **2006**, *110*, 9783−9787.

(16) Calle-Vallejo, F.; Díaz-Morales, O. A.; Kolb, M. J.; Koper, M. T. M. Why is bulk thermochemistry a good descriptor for the electrocatalytic activity of transition metal oxides? *ACS Catal.* **2015**, *5*, 869−873.

(17) Rao, R. R.; Kolb, M. J.; Halck, N. B.; Pedersen, A. F.; Mehta, A.; You, H.; Stoerzinger, K. A.; Feng, Z.; Hansen, H. A.; Zhou, H.; et al. Towards identifying the active sites on RuO_2 (110) in catalyzing oxygen evolution. *Energy Environ. Sci.* **2017**, *10*, 2626−2637.

(18) Man, I. C.; Su, H.-Y.; Calle-Vallejo, F.; Hansen, H. A.; Martínez, J. I.; Inoglu, N. G.; Kitchin, J.; Jaramillo, T. F.; Nørskov, J. K.; Rossmeisl, J. Universality in oxygen evolution electrocatalysis on oxide surfaces. *ChemCatChem* **2011**, *3*, 1159−1165.

(19) Nørskov, J. K.; Rossmeisl, J.; Logadottir, A.; Lindqvist, L.; Kitchin, J. R.; Bligaard, T.; Jonsson, H. Origin of the overpotential for oxygen reduction at a fuel-cell cathode. *J. Phys. Chem. B* **2004**, *108*, 17886−17892.

(20) Siahrostami, S.; Vojvodic, A. Influence of adsorbed water on the oxygen evolution reaction on oxides. *J. Phys. Chem. C* **2015**, *119*, 1032−1037.

(21) Grimaud, A.; Diaz-Morales, O.; Han, B.; Hong, W. T.; Lee, Y.-L.; Giordano, L.; Stoerzinger, K. A.; Koper, M. T.; Shao-Horn, Y. Activating lattice oxygen redox reactions in metal oxides to catalyse oxygen evolution. *Nat. Chem.* **2017**, *9*, 457.

(22) Fabbri, E.; Schmidt, T. J. Oxygen evolution reaction - the enigma in water electrolysis. *ACS Catal.* **2018**, *8*, 9765−9774.

(23) Geiger, S.; Kasian, O.; Ledendecker, M.; Pizzutilo, E.; Mingers, A. M.; Fu, W. T.; Diaz-Morales, O.; Li, Z.; Oellers, T.; Fruchter, L.; et al. The stability number as a metric for electrocatalyst stability benchmarking. *Nat. Catal.* **2018**, *1*, 508−515.

(24) Tsuji, E.; Imanishi, A.; Fukui, K.-i.; Nakato, Y. Electrocatalytic activity of amorphous RuO_2 electrode for oxygen evolution in an aqueous solution. *Electrochim. Acta* **2011**, *56*, 2009−2016.

(25) Willinger, E.; Massué, C.; Schlogl, R.; Willinger, M. G. Identifying key structural features of IrO_x water splitting catalysts. *J. Am. Chem. Soc.* **2017**, *139*, 12093−12101.

(26) Li, T.; Kasian, O.; Cherevko, S.; Zhang, S.; Geiger, S.; Scheu, C.; Felfer, P.; Raabe, D.; Gault, B.; Mayrhofer, K. J. J. Atomic-scale insights into surface species of electrocatalysts in three dimensions. *Nat. Catal.* **2018**, *1*, 300.

(27) Klyukin, K.; Zagalskaya, A.; Alexandrov, V. Ab initio thermodynamics of iridium surface oxidation and oxygen evolution reaction. *J. Phys. Chem. C* **2018**, *122*, 29350−29358.

(28) Tkalych, A. J.; Zhuang, H. L.; Carter, E. A. A Density functional plus U assessment of oxygen evolution reaction mechanisms on β-NiOOH. *ACS Catal.* **2017**, *7*, 5329−5339.

DOI: 10.1021/acs.jpcc.9b03418
J. Phys. Chem. C 2019, 123, 22151−22157

(29) Kresse, G.; Furthmüller, J. Efficiency of ab-initio total energy calculations for metals and semiconductors using a plane-wave basis set. *Comput. Mater. Sci.* **1996**, *6*, 15−50.
(30) Kresse, G.; Furthmüller, J. Efficient iterative schemes for ab initio total-energy calculations using a plane-wave basis set. *Phys. Rev. B* **1996**, *54*, 11169.
(31) Perdew, J. P.; Burke, K.; Ernzerhof, M. Generalized gradient approximation made simple. *Phys. Rev. Lett.* **1996**, *77*, 3865.
(32) Zhang, Y.; Yang, W. Comment on "Generalized gradient approximation made simple". *Phys. Rev. Lett.* **1998**, *80*, 890.
(33) Blöchl, P. E. Projector augmented-wave method. *Phys. Rev. B* **1994**, *50*, 17953.
(34) Kresse, G.; Joubert, D. From ultrasoft pseudopotentials to the projector augmented-wave method. *Phys. Rev. B* **1999**, *59*, 1758.
(35) Grimme, S.; Antony, J.; Ehrlich, S.; Krieg, H. A consistent and accurate ab initio parametrization of density functional dispersion correction (DFT-D) for the 94 elements H-Pu. *J. Chem. Phys.* **2010**, *132*, No. 154104.
(36) Grimme, S.; Ehrlich, S.; Goerigk, L. Effect of the damping function in dispersion corrected density functional theory. *J. Comput. Chem.* **2011**, *32*, 1456−1465.
(37) Briquet, L. G.; Sarwar, M.; Mugo, J.; Jones, G.; Calle-Vallejo, F. A new type of scaling relations to assess the accuracy of computational predictions of catalytic activities applied to the oxygen evolution reaction. *ChemCatChem* **2017**, *9*, 1261−1268.
(38) Bucko, T. Ab initio calculations of free-energy reaction barriers. *J. Phys.: Condens. Matter* **2008**, *20*, No. 064211.
(39) Leung, K. First-principles modeling of Mn (II) migration above and dissolution from $Li_xMn_2O_4$ (001) surfaces. *Chem. Mater.* **2017**, *29*, 2550−2562.
(40) Benedek, R. Role of disproportionation in the dissolution of Mn from lithium manganate spinel. *J. Phys. Chem. C* **2017**, *121*, 22049−22053.
(41) Klyukin, K.; Rosso, K. M.; Alexandrov, V. Iron dissolution from goethite (α-FeOOH) surfaces in water by ab initio enhanced free-energy simulations. *J. Phys. Chem. C* **2018**, *122*, 16086−16091.
(42) Intan, N. N.; Klyukin, K.; Alexandrov, V. Ab initio modeling of transition metal dissolution from the $LiNi_{0.5}Mn_{1.5}O_4$ cathode. *ACS Appl. Mater. Interfaces* **2019**, No. 11, 20110−20116.
(43) Fishman, M.; Zhuang, H. L.; Mathew, K.; Dirschka, W.; Hennig, R. G. Accuracy of exchange-correlation functionals and effect of solvation on the surface energy of copper. *Phys. Rev. B* **2013**, *87*, No. 245402.
(44) Henkelman, G.; Arnaldsson, A.; Jonsson, H. A fast and robust algorithm for Bader decomposition of charge density. *Comput. Mater. Sci.* **2006**, *36*, 354−360.
(45) Reiss, H.; Heller, A. The absolute potential of the standard hydrogen electrode: a new estimate. *J. Phys. Chem.* **1985**, *89*, 4207−4213.
(46) Dickens, C. F.; Norskov, J. K. A Theoretical investigation into the role of surface defects for oxygen evolution on RuO_2. *J. Phys. Chem. C* **2017**, *121*, 18516−18524.
(47) Fabbri, E.; Habereder, A.; Waltar, K.; Kötz, R.; Schmidt, T. J. Developments and perspectives of oxide-based catalysts for the oxygen evolution reaction. *Catal. Sci. Technol.* **2014**, *4*, 3800−3821.
(48) Kötz, R.; Lewerenz, H.; Stucki, S. XPS studies of oxygen evolution on Ru and RuO_2 anodes. *J. Electrochem. Soc.* **1983**, *130*, 825−829.
(49) Zakaryan, H. A.; Kvashnin, A. G.; Oganov, A. R. Stable reconstruction of the (110) surface and its role in pseudocapacitance of rutile-like RuO_2. *Sci. Rep.* **2017**, *7*, No. 10357.
(50) Lyons, M. E.; Floquet, S. Mechanism of oxygen reactions at porous oxide electrodes. Part 2 Oxygen evolution at RuO_2, IrO_2 and $Ir_xRu_{1-x}O_2$ electrodes in aqueous acid and alkaline solution. *Phys. Chem. Chem. Phys.* **2011**, *13*, 5314−5335.
(51) Doyle, R. L.; Godwin, I. J.; Brandon, M. P.; Lyons, M. E. Redox and electrochemical water splitting catalytic properties of hydrated metal oxide modified electrodes. *Phys. Chem. Chem. Phys.* **2013**, *15*, 13737−13783.
(52) Macounova, K.; Makarova, M.; Krtil, P. Oxygen evolution on nanocrystalline RuO_2 and $Ru_{0.9}Ni_{0.1}O_{2-\delta}$ electrodes - DEMS approach to reaction mechanism determination. *Electrochem. Commun.* **2009**, *11*, 1865−1868.
(53) Liu, Y.; Liang, X.; Gu, L.; Zhang, Y.; Li, G.-D.; Zou, X.; Chen, J.-S. Corrosion engineering towards efficient oxygen evolution electrodes with stable catalytic activity for over 6000 hours. *Nat. Commun.* **2018**, *9*, No. 2609.

DOI: 10.1021/acs.jpcc.9b03418
J. Phys. Chem. C 2019, 123, 22151−22157